Revision 2: MS# 5095

High-pressure compressibility and phase stability of Mn-dolomite (kutnohorite)

Sarah E.M. Palaich[1], Robert A. Heffern[1], Anke Watenphul[1], Jason Knight[2], Abby Kavner[1]

[1]Department of Earth, Planetary and Space Sciences, University of California, Los Angeles, CA 90095

[2]Advanced Light Source, Lawrence Berkeley Laboratory, Berkeley, CA 94720

Abstract

We measured the bulk modulus and phase stability of a natural Mn-dolomite, kutnohorite, to 19 GPa. At room temperature, kutnohorite is stable in the rhombohedral dolomite phase up to 19 GPa, with an isothermal bulk modulus of 85(6) GPa (K' = 4). The compressibility of kutnohorite is found to match well with both single and double carbonate trends with respect to bulk modulus and unit cell volume. The thermoelastic properties measured in this study show that the Mn dolomite end member fits well with the systematic of all the rhombohedral carbonates, both calcite (single carbonate) and dolomite (double carbonate) type.

Introduction

Carbon in the deep Earth consists of a primordial component plus carbonate that has recycled into the Earth's mantle via subduction zones (Dasgupta and Hirschmann 2010). Carbon has limited solubility in mantle silicates and therefore exists as carbon-rich accessory phases, either as oxidized carbonate or reduced graphite/diamond/carbide (Shcheka, et al. 2006). Therefore studying the high-pressure behavior of carbonate phases helps determine the role of the Earth's deep interior in the deep carbon cycle. In this paper, we present the high-pressure behavior of kutnohorite, an Mn-rich dolomite, and use the new data in conjunction with existing data to analyze the high pressure behavior of a series of rhombohedral carbonate phases.

Recent experimental studies demonstrate that dolomite, $(CaMg_{1-x}M_x)(CO_3)_2$, where M = Fe, Mn, Zn, undergoes a series of phase transformations with increasing pressures and temperatures. Dolomite I (rhombohedral *R*-3) is the ambient pressure phase. Dolomite II (triclinic P-1) was observed at ambient temperatures and pressures above ~20 GPa (Santillán et al. 2003; Mao et al. 2011; Merlini et al. 2012). A third dolomite phase, Dolomite III, was recently observed in $Ca(Mg_{0.92}Fe_{0.08})(CO_3)_2$ by Mao, et al. (2011) and $Ca(Mg_{0.6}Fe_{0.4})(CO_3)_2$ by Merlini, et al. (2012), by compressing above 35 GPa and laser heating. This dolomite III phase is stable during temperature-quench, allowing Merlini et al. to refine a structure (triclinic *P*-1). These results raise the possibility of a dolomite-structured carbonate that may be stable at the high-pressures and high-temperatures of the lower mantle and motivate our study to expand the compositional range to include the Mn end-member dolomite, kutnohorite.

Experimental Methods

Our starting sample was kutnohorite from Franklin, NJ with a composition of $(Ca_{0.76}Mn_{0.24})Mn(CO_3)_2$ and with ~5% rhodochrosite ($MnCO_3$) vein impurities, determined by electron microprobe. This Mn-enriched composition is in agreement with a previous determination by Frondel and Bauer (1955) and is not unusual for kutnohorite from Franklin, NJ. In addition, the Mn excess does not affect the structure of the kutnohorite, which is the dolomite structure comprised of alternating layers of cations interspaced with layers of carbonate triangles. Pieces of whole rock were ground and then mixed with 5-10 wt% Au, which was used an internal X-ray pressure calibrant (Takemura and Dewaele 2008).

Two separate diamond anvil cell experiments were performed, each gas-loaded with Ne to ensure hydrostatic pressure and including a small ruby chip for cross-reference pressure measurement (Rivers et al. 2008). In a first experiment, the kutnohorite-Au mixture was pressed, sandwiched between NaCl chips and then placed in a 150 x 70 μm hole in a pre-indented rhenium gasket in a diamond anvil cell equipped with 500 μm culets. This sample was compressed at room temperature to 19 GPa in steps of 3-5 GPa (Figure 1). A second diamond anvil cell equipped with 300 μm culets was loaded with prepressed kutnohorite-Au mixture placed in an 80 x 50 μm gasket hole with no NaCl calibrant. A verification X-ray diffraction pattern was taken at 0.5 GPa before this sample was compressed to 35 GPa and then laser-heated with the double-sided fiber laser heating system (Clark et al. 2012).

Angle-dispersive X-ray diffraction data was collected on a MAR345 image plate at an energy of 28 KeV (0.4428 Å) at beamline 12.2.2 at the Advanced Light Source,

Lawrence Berkeley National Laboratory. All diffraction patterns were integrated using GSAS II to display intensity versus two-theta angles (Toby and Von Dreele 2013).

Up to 19 GPa kutnohorite, Au and NaCl were indexed and both Rietveld Refinement methods (GSAS) and Gaussian fits to each of the diffraction peaks were used to find extract pressure-volume information. Pressure was measured before and after each pressure step using ruby fluorescence, and determined from an internal calibrant using the lattice volume of the Au determined by the X-ray patterns and fitting to the equation of state of Au (Takemura and Dewaele 2008). Pressure error values were propagated from the uncertainty in the refinement fit to the Au lattice parameters. The second loading of kutnohorite did not include the NaCl and the kutnohorite starting structure was confirmed with a diffraction pattern obtained at 0.5 GPa after gas loading but before compression and heating (Figure 1). The patterns collected above 35 GPa show a change in the structure, indicating a change from the initial rhombohedral structure. While the pressure of the transformation is similar to the dolomite III transformation observed in the Mg and Fe-bearing dolomites, it is not clear from our current diffraction patterns whether the structures are related.

Results and Discussion

Upon compression in the diamond cell, we find kutnohorite to be stable in the dolomite I structure to 19 GPa at ambient temperature (300 K). For each diffraction pattern the best-fit rhombohedral lattice parameters were determined from Gaussian fits of each indexed peak and by Reitveld refinement (Figure 2). Although the error bars are much greater for the individual Gaussian fits, the volume data extracted from each method is nearly indistinguishable. As illustrated in Table 1 and Figure 2, the large

Gaussian fit volume error originates from an under constraint of lattice parameter *c*. The available peaks in our two-theta range constrained the lattice parameter *a* much better. The *c*/*a* ratio of kutnohorite at 0.3 GPa is 3.366, similar to 3.354 found by Graf (1961). The ratio steadily decreases with increasing pressure, lowering to 3.105 at 20 GPa, which is consistent with a more compressible *c* axis.

As shown in Figure 2, the best-fit of the pressure-volume data to a 2nd order Birch-Murnaghan equation of state (with $K'_{T,0}$ fixed at 4) yields an isothermal bulk modulus of 85(6) GPa and a V_0 of 332(2). A 3rd order fit is also shown in Figure 2 that yields a bulk modulus of 110(1) GPa, K' = 1.9(1) and V_0 of 329.3(1). This study does not include sufficient data points to merit the use of this higher order equation of state. A later ambient-pressure single-crystal measurement was performed on the same sample and confirmed the dolomite I structure with a unit cell volume of 230(1) Å^3, which is consistent with our fitted results. These ambient volumes are within the previous range of literature values (330-336 Å^3) that depend on disorder (Graf 1961; Farkas et al. 1988). The powder diffraction result is likely the average of many differently disordered crystallites, which would account for the disparity between the single crystal and powder diffraction results. This bulk modulus found in the 2nd order equation of state fit is comparable to those of Fe dolomite-type end-member ankerite, 91 GPa, and dolomite, 94 GPa (Ross and Reeder, 1992).

The compressibility-volume systematics of Mg, Fe and Mn-dolomite can be directly compared with other rhombohedral carbonates such as calcite ($CaCO_3$). These rhombohedral carbonates have been previously investigated under pressure in some detail (Ross 1997; Zhang et al. 1997; Zhang and Reeder 1999; Ono 2007; Litasov et al. 2013).

In the rhombohedral carbonates, the marginally distorted cation octahedra are corner-linked through shared oxygen anions of carbonate groups. These carbonate planar triangles are the most incompressible elements in the structure. Studies by Ross (1997) and Ross and Reeder (1992) illustrate that the M-O-M and M-O-C angles in magnesite, dolomite and ankerite have very little variation with pressure. This means bond bending is not a major process in the compression of the rhombohedral carbonates. The cation range of these carbonates encompasses divalent alkaline earth elements, 3d transition metals and 4d transition metals ranging in size from 0.69 to 1.0 Å. The dolomite structure is a double carbonate and thus combines at least two different cations from this list, with one always being Ca^{2+}, in alternating cation layers. The composition of our kutnohorite sample, $(Ca_{0.76}Mn_{0.24})Mn(CO_3)_2$, shows a significant excess of manganese, raising the possibility that it is not ordered like a standard dolomite, but perhaps mixes Ca and Mn between the two layers.

In kutnohorite the compressibility of the unit cell is controlled primarily by the behavior of the Ca and Mn octahedra since the carbonate planar triangles are essentially incompressible in this pressure regime. This leads to anisotropic compression in all of the rhombohedral carbonates as evidenced by a significantly more compressible *c* axis. A linear relationship is predicted between the bulk moduli and the ambient unit cell volume. Figure 3 shows this trend for the rhombohedral carbonates. The deviation of $MgCO_3$ and $CdCO_3$ from the linear trend is of note. The higher compressibility of $MgCO_3$ is attributed to substantially higher *a*-axis compressibility than found in the other rhombohedral carbonates of similar ambient volume (i.e. $CoCO_3$ and $ZnCO_3$) (Zhang and

Reeder 1999). Indeed, Zhang and Reeder (1999) found a linear relationship between *c*-axis compressibility and M-O bond length for all cation types.

Our new kutnohorite data fit within the linear relationship described by the rhombohedral carbonates (Figure 3). The dolomites have higher volumes and lower bulk moduli, and fall on a trend line of -0.60(20) GPa/Å^3 while the calcite-type carbonates show a slope of -0.61(3) GPa/Å^3, excluding the magnesite and otavite ($CdCO_3$) data points. In addition, unit cell volumes increase as the cation changes from Mg > Fe > Mn, both in the single and double carbonate series, consistent with other transition metal systematics within mineral structures. Depending on the new bonding environment high pressure polymorphs of dolomite might be expected to follow this linear trend since the elastic behavior of the structure is rooted in the constituent polyhedral compressibility and size of the cation sites.

Implications for dolomite structures

This work provides new measurements of the isothermal bulk modulus of kutnohorite, which is found to be 85(6) GPa. This is the first instance of this bulk thermoelastic property of kutnohorite being reported in the literature and we find it in good agreement with other bulk moduli found for ankerite and dolomite. The similarity to the bulk moduli in other dolomite end members suggests that compositional variation in the dolomites does not affect structural evolution. We have also found that the Mn end member of dolomite undergoes a change at high pressure (35 GPa) and temperature that may be in accordance with previous work done on Fe-bearing dolomites by Mao et al. (2011) and Merlini et al. (2012). This finding has the important implication that dolomite may undergoes phase transitions regardless of composition and that these changes are

perhaps inherent to the dolomite structure. In the unlikely case that a carbonate with dolomite stoichiometry is preserved in a cold subducting slab these results imply the dolomite will be stable at the P,T conditions of the lower mantle. Finally, we have highlighted the systematics of single and double rhombohedral carbonates. The compressional and structural characteristics of these minerals are linearly related for both single and double carbonates, implying that the compressibility of the constituent cation polyhedra governs the bulk compressibility of these rhombohedral carbonates. We hypothesize that the linear trend between compressibility and structure will continue in the high-pressure dolomite structures, but further study is needed to gain information on the structure and bulk thermoelastic properties of the high pressure forms of dolomite.

Acknowledgements

This work was funded in part by the DOE DE-FG02-10ER16136 and NSF EAR-0969033. Portions of this work were performed at Beamline 12.2.2, Advanced Light Source, Lawrence Berkeley National Laboratory, supported by the Department of Energy under contract No. DE-AC02-05CH1231 and COMPRES, the Consortium for Materials Properties Research in Earth Sciences, under NSF Cooperative Agreement EAR 10-43050. We thank Marco Merlini for conversations about high-pressure dolomite structures.

References

Clark, S.M., MacDowell, A.A., Knight, J., Kalkan, B. Yan, J., Chen, B., and Williams, Q. (2012) Beamline 12.2.2: An Extreme Conditions Beamline at the Advanced Light Source. Synchrotron Radiation News, 25, 10-11.

Dasgupta, R., and Hirschmann, M.M. (2010) The deep carbon cycle and melting in Earth's interior. Earth and Planetary Science Letters, 298, 1–13.

Farkas, L., Bolzenius, B.H., Shafer, W., and Will, G. (1988) The crystal structure of kutnohorite $CaMn(CO_3)_2$. Neues Jahrbuch für Mineralogie Monatshefte, 12, 539-546.

Frondel, C., and Bauer, L.H. (1955) Kutnahorite: A manganese dolomite: $CaMn(CO_3)_2$: American Mineralogist, 40, 748–760.

Graf, D.L. (1961) Crystallographic tables for the rhombohedral carbonates. American Mineralogist, 46, 1283-1316.

Larson, A.C., and Von Dreele, R.B. (2000) General Structure Analysis System (GSAS). Los Alamos National Laboratory Report LAUR, 86-748.

Litasov, K.D., Shatskiy, A., Gavryushkin, P.N., Sharygin, I.S., Dorogokupets, P.I., Dymshits, A.M., Ohtani, E., Higo, Y., and Funakoshi, K. (2013) P-V-T equation of state of siderite to 33 GPa and 1673K. Physics of the Earth and Planetary Interiors, 224, 83–87.

Mao, Z., Armentrout, M., Rainey, E., Manning, C.E., Dera, P., Prakapenka, V.B., and Kavner, A. (2011) Dolomite III: A new candidate lower mantle carbonate.

Geophysical Research Letters, 38, L22303.

Merlini, M., Crichton, W.A., Hanfland, M., Gemmi, M., Muller, H., Kupenko, I., and Dubrovinsky, L. (2012) Structures of dolomite at ultrahigh pressure and their influence on the deep carbon cycle. Proceedings of the National Academy of Sciences, 109, 13509–13514.

Merlini, M., Hanfland, M., and Crichton, W.A. (2012b) $CaCO_3$-III and $CaCO_3$-VI, high pressure polymorphs of calcite: Possible host structures for carbon in the Earth's mantle. Earth and Planetary Science Letters, 333-334, 265-271.

Morlidge, M., Pawley, A. and Droop, G. (2006) Double Carbonate breakdown reactions at high pressures: an experimental study in the system CaO-MgO-FeO-MnO-CO_2. Contributions to Mineralogy and Petrology, 152, 365-373.

Ono, S. (2007) High pressure phase transformation in $MnCO_3$: a synchrotron XRD study. Mineralogical Magazine, 71, 105-111.

Rivers, M., Prakapenka, V.B., Kubo, A., Pullins, C., Holl, C.M., and Jacobsen, S.D. (2008) The COMPRES/GSECARS gas-loading system for diamond anvil cells at the Advanced Photon Source. High Pressure Research, 28, 273-292.

Ross, N.L. (1997) The equation of state and high-pressure behavior of magnesite. American Mineralogist, 82, 682-688.

Ross, N.L., and Reeder, R.J. (1992) High-pressure structural study of dolomite and ankerite. American Mineralogist, 77, 412–421.

214 Santillán, J., Williams, Q., and Knittle, E. (2003) Dolomite-II: A high-pressure
215 polymorph of $CaMg(CO_3)_2$: Geophysical Research Letters, 30, 1054.

216 Shcheka, S.S., Wiedenbeck, M., Frost, D.J., and Keppler, H. (2006) Carbon solubility in
217 mantle minerals. Earth and Planetary Science Letters, 245, 730-742.

218 Takemura, K. and Dewaele, A. (2008) Isothermal equation of state for gold with a He-
219 pressure medium. Physics Review B, 78, 104119.

220 Toby, B.H. (2001) EXPGUI, a graphical user interface for GSAS. Journal of Applied
221 Crystallography, 34, 210-213.

222 Toby, B.H., and Von Dreele, R.B. (2013) GSAS-II: the genesis of a modern open-source
223 all purpose crystallography software package. Journal of Applied Crystallography,
224 46, 544-549.

225 Zhang, J., Martinez, I., Guyot, F., Gillet, P., and Saxena, S.K. (1997) X-ray diffraction
226 study of magnesite at high pressure and high temperature. Physics and Chemistry of
227 Minerals, 24, 122-130.

228 Zhang, J., and Reeder, R.J. (1999) Comparative compressibilities of calcite-structure
229 carbonates: Deviations from empirical relations. American Mineralogist, 84, 861–
230 870.

231

232

233 Tables and Captions:

Kutnohorite Fitted Peaks			Kutnohorite GSAS Refinement			Au GSAS Refinement			
a	*c*	Volume	*a*	*c*	Volume	*a*	Volume	Pressure	R_{wp}
4.834(25)	16.27(13)	329(5)	4.843(1)	16.239(4)	329.93(9)	4.0749(1)	67.663(7)	0.46409(2)	0.0746
4.854(24)	16.21(18)	330(4)	4.8524(9)	16.173(4)	329.81(6)	4.0735(3)	67.594(17)	0.63728(2)	0.0456
4.799(30)	15.64(16)	312(5)	4.8161(15)	15.691(6)	315.20(15)	4.0399(5)	65.939(22)	5.1245(14)	0.0591
4.77(2)	15.40(13)	303(4)	4.7704(7)	15.404(5)	303.58(9)	4.0118(2)	64.569(13)	9.3701(16)	0.0777
4.751(24)	15.19(18)	297(5)	4.761(3)	15.176(20)	297.94(35)	3.9990(7)	63.965(32)	11.413(5)	0.0639
4.737(21)	14.98(22)	291(5)	4.751(3)	14.957(14)	292.47(20)	3.9744(3)	62.741(15)	15.905(3)	0.0549
4.712(27)	14.63(17)	281(5)	*	*	*	3.9562(3)	61.922(17)	19.197(5)	0.0834

234

235 Table 1. Room temperature kutnohorite and Au unit cell parameters to 20 GPa from both
236 GSAS refinements and Gaussian peak fitting. Note that the highest pressure refinement
237 was not able to determine the kutnohorite parameters and thus the peak fitting data point
238 is used in our analysis.

5. Figure Captions

Figure 1. Diffraction patterns of kutnohorite to 19 GPa. Bottom pattern shows Au mixture used in the second high pressure experiments at 0.5 GPa before compression and heating. Other patterns were loaded with Au mixture and sandwiched between NaCl flakes. Rhombohedral kutnohorite is present to 20 GPa. The starred peaks represent an unidentified cubic phase.

Figure 2. The unit cell volume of kutnohorite as a function of pressure as determined by both Rietveld Refinement (dark circles) and Gaussian peak fitting (final diamond point). Volume error bars for the Gaussian fit point reflect that the indexed peaks better constrain unit cell parameter *a* than *c*. For our equation of state fitting we used the refinement results except at the highest pressure where no refinement was possible and we used the Gaussian peak fitting result (19.2 GPa data point). Equation of state fit to the kutnohorite pressure-volume data as determined from both a 2^{nd} and 3^{rd} order Birch Murnaghan equation of state are shown.

Figure 3. Calcite-type carbonate data and dolomite data examining the relationship between bulk modulus (GPa) and ambient unit cell volume ($Å^3$). The dolomites fall on a trend line of -0.6(2) GPa/$Å^3$ while the calcite-type carbonates exhibit a slope of -0.61(3) GPa/$Å^3$.

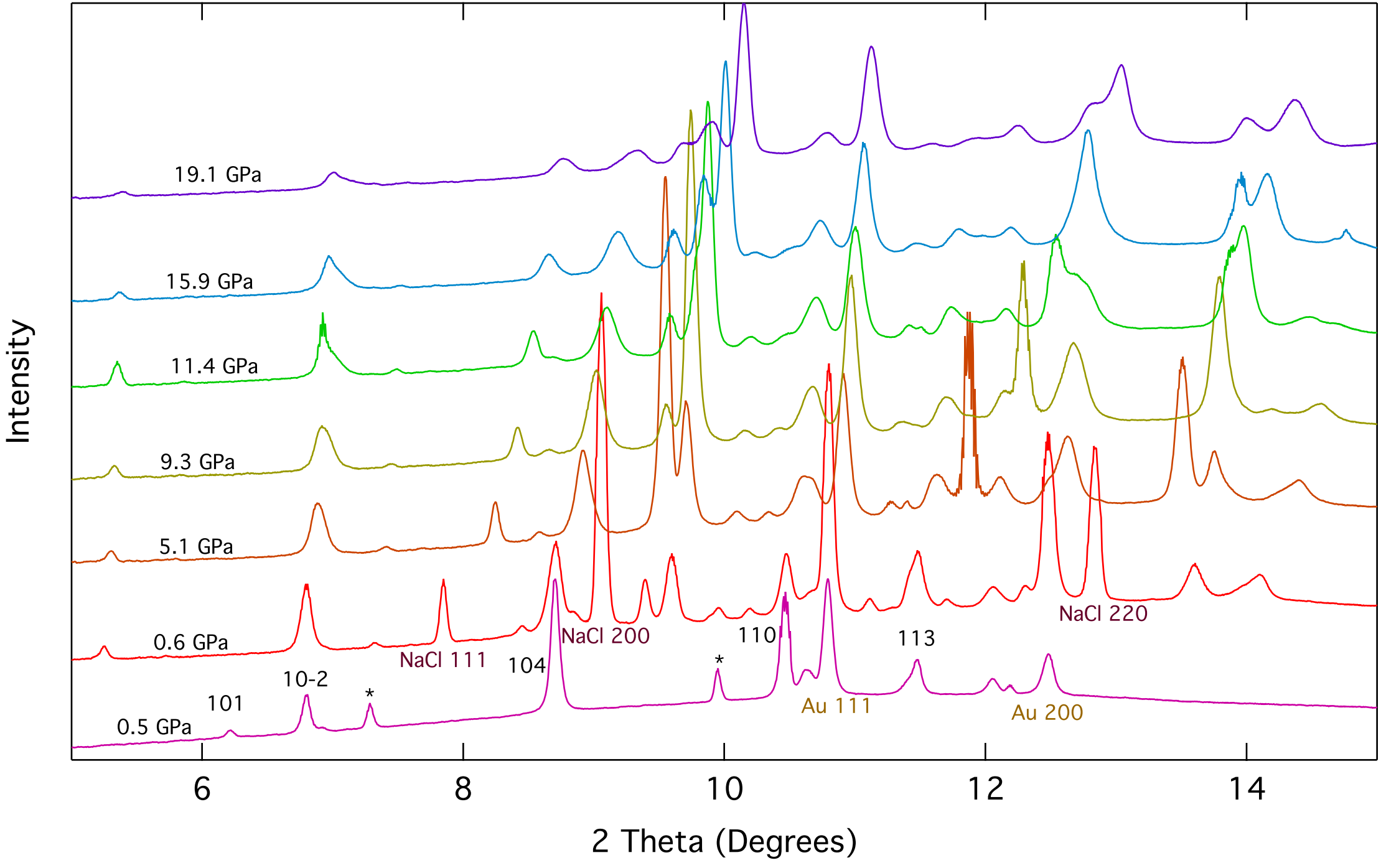
19.1 GPa
15.9 GPa
11.4 GPa
9.3 GPa
5.1 GPa
0.6 GPa
0.5 GPa
101
10-2
*
NaCl 111
104
NaCl 200
*
110
Au 111
113
NaCl 220
Au 200
Intensity
6
8
10
12
14
2 Theta (Degrees)

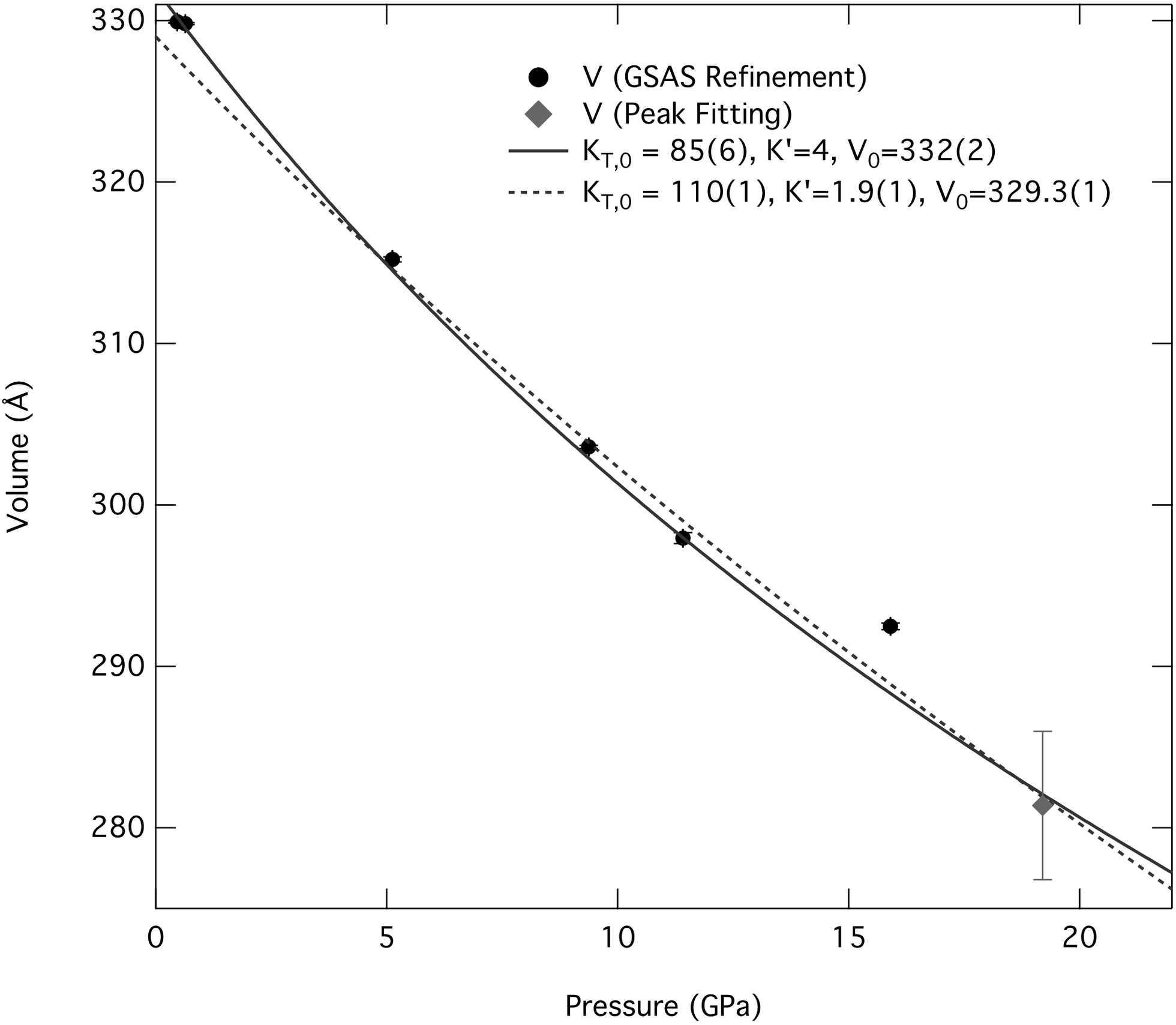
V (GSAS Refinement)
V (Peak Fitting)
K$_{T,0}$ = 85(6), K'=4, V$_0$=332(2)
K$_{T,0}$ = 110(1), K'=1.9(1), V$_0$=329.3(1)
Volume (Å)
Pressure (GPa)
330
320
310
300
290
280
0
5
10
15
20

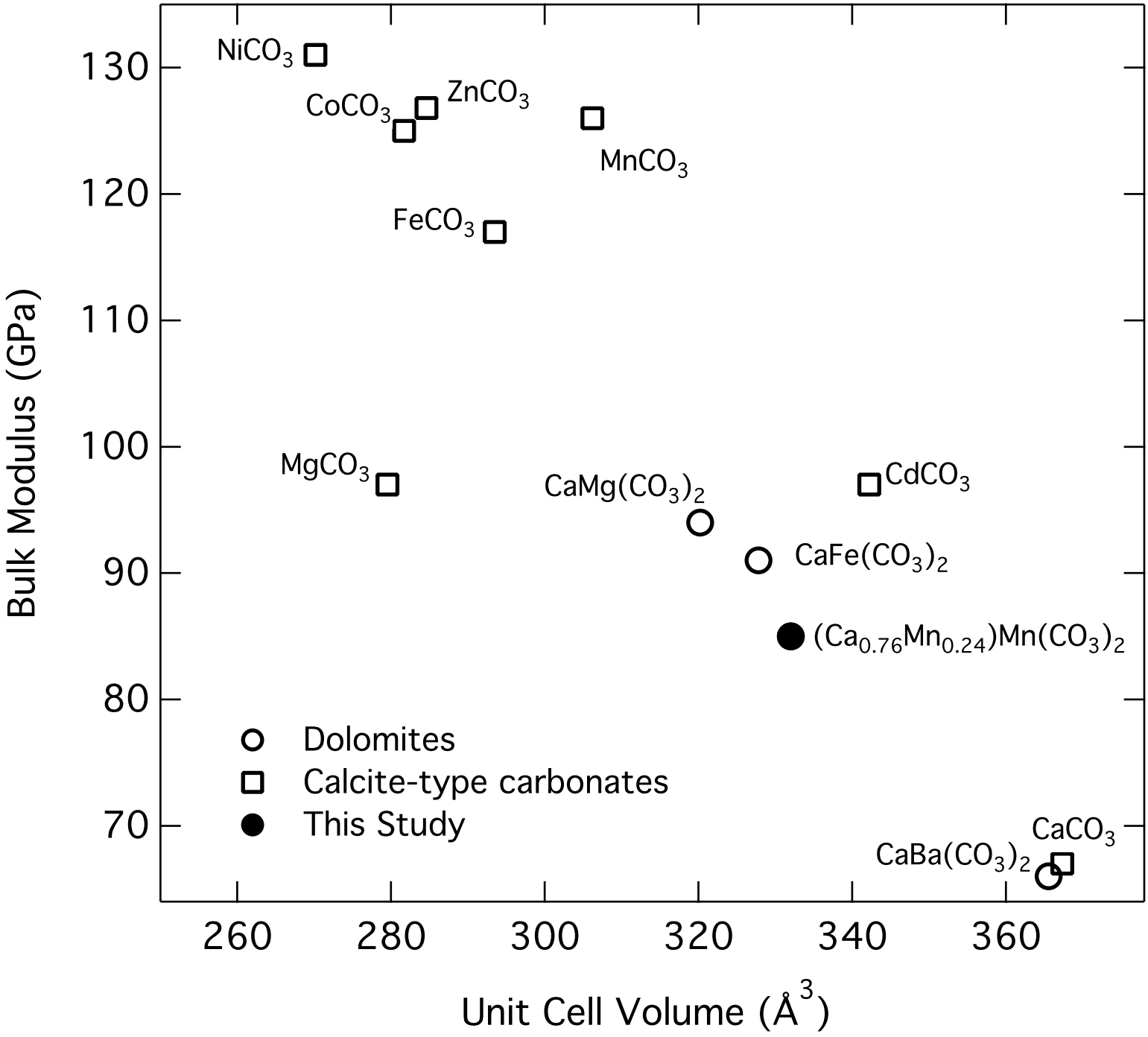
NiCO3
CoCO3
ZnCO3
MnCO3
FeCO3
MgCO3
CaMg(CO3)2
CdCO3
CaFe(CO3)2
(Ca0.76Mn0.24)Mn(CO3)2
CaCO3
CaBa(CO3)2
Dolomites
Calcite-type carbonates
This Study
Bulk Modulus (GPa)
Unit Cell Volume (Å3)
130
120
110
100
90
80
70
260
280
300
320
340
360

Kutnohorite Fitted Peaks			Kutnohorite GSAS Refinement			Au GSAS Refinement			
a	*c*	Volume	*a*	*c*	Volume	*a*	Volume	Pressure	Rwp
4.834(25)	16.27(13)	329(5)	4.843(1)	16.239(4)	329.93(9)	4.0749(1)	67.663(7)	0.46409(2)	0.0746
4.854(24)	16.21(18)	330(4)	4.8524(9)	16.173(4)	329.81(6)	4.0735(3)	67.594(17)	0.63728(2)	0.0456
4.799(30)	15.64(16)	312(5)	4.8161(15)	15.691(6)	315.20(15)	4.0399(5)	65.939(22)	5.1245(14)	0.0591
4.77(2)	15.40(13)	303(4)	4.7704(7)	15.404(5)	303.58(9)	4.0118(2)	64.569(13)	9.3701(16)	0.0777
4.751(24)	15.19(18)	297(5)	4.761(3)	15.176(20)	297.94(35)	3.9990(7)	63.965(32)	11.413(5)	0.0639
4.737(21)	14.98(22)	291(5)	4.751(3)	14.957(14)	292.47(20)	3.9744(3)	62.741(15)	15.905(3)	0.0549
4.712(27)	14.63(17)	281(5)	*	*	*	3.9562(3)	61.922(17)	19.197(5)	0.0834